Chapter 5
Reactor antineutrino background in geoneutrino measurements

Barbara Ricci and Marica Baldoncini

Abstract Reactor antineutrinos represent the most important source of background in geoneutrinos detection. An updated estimate of reactor antineutrino signal all over the world, with particular attention on the geographical sites for existing and future geoneutrino experiments, is presented here. In the calculation, the most recent data on Thermal Power for each nuclear plant, on reactor antineutrino spectra and on three neutrino oscillation mechanism are taken into account.

5.1 Introduction

Antineutrinos from the decay chains of ^{238}U and ^{232}Th existing in the Earth interior (the so called geoneutrinos) have been recently detected both by KamLAND [1] and by Borexino [2] experiments, throught the inverse beta decay:

$$\bar{\nu}_e + p \rightarrow n + e^+ \qquad E_{th} = 1.806 \quad \text{MeV} \quad . \tag{5.1}$$

Future experiments for geoneutrinos detection have been proposed (or are starting) in several location in the world, for instance: SNO+ in Canada [3], LENA project in Europe [4], Hawaii Anti-Neutrino Observatory[5] in USA and JUNO experiment in China [6]. Moreover, LENA and JUNO would provide a substantial increase of the detection sensitivity and of the event rate thanks to their larger target masses (50 kton and 20 kton, respectively) compared to the 1 kton scintillator mass of KamLAND and SNO+ and to the 0.3 kton of Borexino.

The main source of background in geoneutrino detection is the production of electron antineutrino by nuclear plants, which are the strongest man-made antineu-

Barbara Ricci
Università di Ferrara and INFN-Ferrara e-mail: `ricci@fe.infn.it`

Marica Baldoncini
Università di Ferrara and INFN-Ferrara e-mail: `baldoncini@fe.infn.it`

trino sources. Many nuclei, produced in the fission process of nuclear fuel, decay through beta processes with the consequent emission of electron antineutrinos, the so called reactor antineutrinos. The energy spectrum of reactor antineutrinos extends up to $\simeq 10$ MeV, well beyond the end point of the geoneutrino spectrum (3.27 MeV). As a consequence, in the geoneutrino energy window, o Low Energy Region, (1.8 - 3.27 MeV) there is an overlap between geoneutrino and reactor antineutrino signals, see Fig. 5.1.
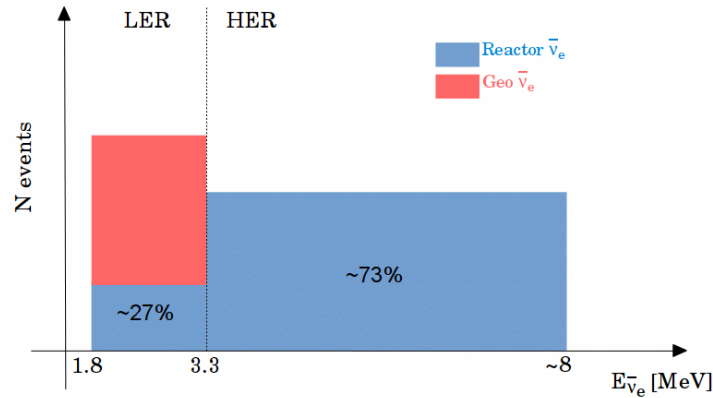
Fig. 5.1 A schematic picture of the expected reactor signal in the Low Energy Region (LER) and in the High Energy Region (HER), courtesy from [9]. The LER is the so called geoneutrino energy window in the text.

Therefore, a careful analysis of the expected reactor antineutrino event rate at a given experimental site is mandatory. In particular, the comparison between the predicted reactor antineutrino signal in the geoneutrino energy window and the expected geoneutrino signal can be considered an important tool to access the potentiality of a geoneutrino detector. Note also that the reactor contribution to the signal changes according to the different reactor operational conditions, while the geoneutrino component is, in principle, time independent.

With this aim, we performed a calculation of reactor antineutrinos signal all over the world with particular attention to the sites of existing and proposed geoneutrino experiments. Previous analyses have been presented, for instance see ref. [7] and [8]. See also [9] for a more detailed discussion on signals and uncertainties.

In this paper, first we illustrate how the reactor antineutrino signal is calculated, next we discuss in detail the main parameters involved in the calculation. Finally we report our results, with particular attention on those sites where geoneutrinos experiments already exist or are planned.

5.2 Reactor antineutrino signal

At present, in the world, there are about 440 nuclear power reactors, providing, nominally, a total amount of about 1160 Thermal GW (corresponding to 380 Electrical GW). With an average energy released per fission given by $\sim$200 MeV and 6 antineutrinos produced along the beta decay chains of the neutron-rich unstable fission products, one has about 10^{20} $\bar{v}/s$ emitted from a reactor with a typical thermal power of 3 GW.
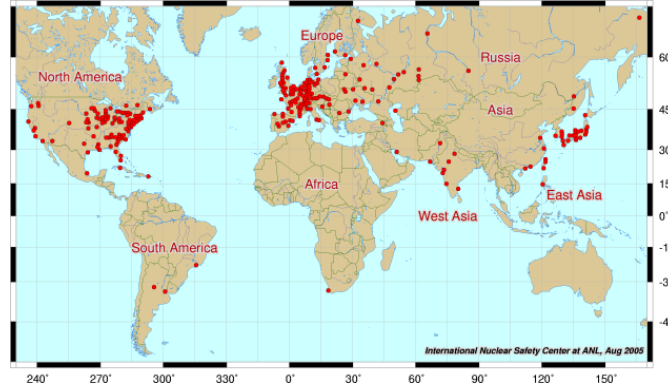
Fig. 5.2 World distribution of nuclear power plants, from ref. [10] .

In order to calculate the expected reactor antineutrino signal one needs several information involving production, propagation and detection of antineutrinos. In this respect, we calculate the reactor antineutrino signal as follows:

$$N_{ev} = \varepsilon N_p \tau \sum_{r=1}^{N_{react}} \frac{P_r}{4\pi L_r^2} <LF_r> \int dE_{\bar{v}_e} \sum_{i=1}^{4} \frac{f_i}{E_i} \lambda_i(E_{\bar{v}_e}) \sigma(E_{\bar{v}_e}) P_{ee}(E_{\bar{v}_e}, L_r, \hat{\theta}) \quad (5.2)$$

where ε is the detector efficiency; N_p is the number of target protons in the detector, τ is period of data taking; index r varies over the N reactors considered, L_r, P_r and $<LF_r>$ are the distance, the nominal thermal power and the averaged (in the period τ) Load Factor of reactor r, respectively. The index i stands for the different components of nuclear fuel; p_i is the power fraction of the fuel component i; Q_i is the energy released per fission from fuel component i; $\lambda(E_{\bar{v}})$ is the antineutrino spectrum originating by the fission of the ith component; $\sigma(E_{\bar{v}})$ is the inverse beta decay cross section; P_{ee} is the survival probability of the reactor antineutrinos of energy $E_{\bar{v}}$ travelling the distance L_r, depending on the neutrino mixing parameters $\hat{\theta}$.

In our calculation we assume a 100% detection efficiency, for a detector containing 10^{32} target protons and operating continuously for 1 year, so that we can express the signal in unit of Terrestrial Neutrino Unit, introduced in [7]: 1 TNU= 1 event/yr/10^{32} target protons. This represents a convenient unit since the typical

scale of a liquid scintillator is of the order of kton ($\simeq 10^{32}$ protons) and data taking period covers some years. Furthermore, TNU unit does not depend on experimental features (chemical composition of the liquid scintillator, fiducial volume...), so one can easily compare the signals expected in different experiments and coming from different sources.

One can see that the several ingredients occurring in the signal calculation, span from nuclear physics (Q_i, $\lambda(E_{\bar{\nu}})$) to neutrino properties (P_{ee}, $\sigma(E_{\bar{\nu}})$), passing through our knowledge of the nuclear plant operation procedure and position (p_i, P_r, L_r). In the following, we present the input data adopted in our calculation, starting from the properties of the nuclear power plants, then we discuss the main nuclear physics inputs and finally we discuss the parameters affecting neutrino survival probability and the neutrino cross section for inverse beta reaction (5.1).

5.3 Nuclear power reactors

Official information on existing nuclear power plants are provided by the Power Reactor Information System (PRIS), developed and maintained by the Interantional Atomic Energy Agency (IAEA) for over four decades [11]. PRIS contains information on reactor specification data (status, operator, owner...) and technical design characteristics. It also includes data on energy production and loss, outage and operational event information. Each year (in summer) PRIS produces documents containing information about the nuclear power reactor performance relative to the previous year. In our calculation we considered the most recent available data about reactors operating in 2013 [12].

5.3.1 Thermal Power and Load Factor

On PRIS documents the "nominal thermal power ", P_r, of each nuclear core is reported. In addition, the reactor operational time profile is reported in term of a Load Factor (LF), which is the percentage quantity expressing the effective working condition of a core in a specific period of the operating cycle. It is defined as the ratio between the net electrical energy produced during a reference period (after subtracting the electrical energy taken by auxiliary units) and net electrical energy that would have been supplied to the grid if the unit were operated continuously at the reference power unit during the whole reference period. Load factor data are published both on a monthly timeline and as an annual average, in our calculation we have considered the last one.

Furthermore, we assume that published values of "electrical" load factors are equal to "thermal" ones, which are not available at present.

In the literature direct measurements of thermal power of some nuclear cores are reported and can reach a sub-percent level accuracy (see e.g. [13]). But we observe

that the regulatory specifications for safe reactor operations for Japan and the United States require, at minimum, an accuracy of 2%. So we adopt a conservative uncertainty of 2% in reactor antineutrino signal due to the thermal power, also with the aim to take into account the error due to our assumption in considering electrical *LF* equal to (unknown) thermal *LF*.

5.3.2 Power and fission fractions

The operating principle of nuclear power reactors lies in the generation of heat by the neutron-induced fission of uranium and plutonium isotopes and by the subsequent decays of unstable fission fragments. In a typical reactor, more than 99.9% of antineutrinos above the energy threshold of beta inverse reaction are emitted in large Q-value beta decays of unstable daughter fragments, that originated in the fission process of just four isotopes: ^{235}U, ^{238}U, ^{239}Pu and ^{241}Pu .

In the literature, the different fuel isotope contributions to the generated thermal power are expressed as fission fractions or as power fractions, which have to be considered as different physical quantities. The fission fraction f_i is defined as a relative fission yield (i.e., as the fraction of fissions produced by the $i-th$ isotope), whereas the power fraction p_i corresponds to the fraction of the total thermal power produced by the fission of the $i-th$ isotope, the relationship being:

$$p_i = \frac{f_i Q_i}{\sum\limits_{i=1}^{4} f_i Q_i} \tag{5.3}$$

where Q_i represents the energy released by the fission of the $i-th$ isotope, see Table 5.2.

During the power cycle of a nuclear reactor, the composition of the fuel changes as Pu isotopes are bred and U is consumed: thus, the power (fission) fractions are time-dependent quantities. Fuel isotope contributions also depend on the burn-up technology adopted in the given reactor core as different core types are characterized by different fuel compositions, which in turn give rise to different isotope contributions to the total thermal power. Several technologies have been developed in the years (see e.g. [14] for an introduction) and we report here some brief outlines.

- Pressurized Water Reactors (PWRs) and Boiling Water Reactors (BWRs), using water both as cooling and moderating materials, require the adoption of enriched uranium as nuclear fuel, with a typical enrichment level of ^{235}U ranging from 2% to 5% . The ∼360 PWR and BWR cores in the world provide ∼81% of the total thermal power.
- About 30 PWRs (mainly located in Europe) use MOX fuel, which is a mix of more than one oxide of fissile material (plutonium recovered from spent nuclear fuel, reprocessed uranium or depleted uranium). Generally, approximately 30%

of the total power of these reactors comes from the MOX fuel, while the remaining 70% of the power is produced by standard PWR fuel.

- Pressurized Heavy Water Reactors (PHWRs) use heavy water as both moderator and coolant. Due to the smaller neutron capture cross section with respect to ordinary water, PHWRs can burn natural uranium. At present 48 PHWRs are operating in the world, producing only ∼7% of the total worldwide thermal power.
- Gas Cooled Reactors (GCRs) and Light Water Graphite Reactors (LWGRs) exploit graphite as moderator, which allows the adoption of lower uranium enrichment levels, typically between 2.2% and 2.7% . These types of reactors (about 30 cores in the world) provide ∼5% of the total thermal power.

In our calculation, PWRs, BWRs, LWGRs and GCRs are assumed to adopt an enriched uranium composition. As we have already mentioned, such composition is not constant 'in space and in time': the fuel composition can vary due to the technological differences among the nuclear plants and due to the different stage of burn up of a single nuclear core. In Table 5.1 we report some different sets of fission fractions found in the literature for uranium enriched compositions. Furthermore, at the moment, we do not know the exact fuel composition used by each core operating in the world. So we assign to all cores, of the type mentioned above, the following representative fission fractions:

$$^{235}\text{U} : {}^{238}\text{U} : {}^{239}\text{Pu} : {}^{241}\text{Pu} = 0.575 : 0.075 : 0.298 : 0.052 \quad . \tag{5.4}$$

Concerning PHWRs, we adopt the corresponding set of power fraction as in [2]:

$$^{235}\text{U} : {}^{238}\text{U} : {}^{239}\text{Pu} : {}^{241}\text{Pu} = 0.542 : 0.0243 : 0.411 : 0.0222 \quad . \tag{5.5}$$

For the cores adopting the MOX fuel, we assume that 30% of their thermal power was originated by the power fractions

$$^{235}\text{U} : {}^{238}\text{U} : {}^{239}\text{Pu} : {}^{241}\text{Pu} = 0.00 : 0.080 : 0.708 : 0.212 \quad , \tag{5.6}$$

again from [2], the remaining 70% of the thermal power originated by the composition as in Eq. (5.4). At our knowledge, no other values of fission fractions for PHWRs and MOX cores are available in the literature.

In order to estimate the error in the calculation due to our "ignorance" of which fission fractions are really present in each nuclear core, we proceed as follows. We calculate the signal assigning to all cores, using enriched uranium fuel, a fixed set of fission fractions; we repeat the calculation for all 18 sets reported in the Table 5.1; finally we compare the signal values, and we calculate the relative variance as: $|MAX - MIN|/(\sqrt{12} \cdot MEAN)$, i.e. we assume a flat distribution of the signals calculated with the different sets of fission fractions. We find an effect of the order of 1% or less, see the third column of Table 5.5. The effect of adopting different sets of fission fractions is smaller for a detector placed in the Sudbury Observatory, due

to the fact that all the nearest nuclear plants adopt PHWRs, for which we consider an unique set of fission fractions.

Table 5.1 Fission fractions, f_i as found in the literature referring to power reactors using enriched uranium fuel. The corresponding references are also indicated.

^{235}U	^{238}U	^{239}Pu	^{241}Pu	ref.
0.538	0.078	0.056	0.328	[17]
0.614	0.074	0.038	0.274	”
0.62	0.074	0.042	0.274	”
0.584	0.068	0.05	0.298	”
0.543	0.07	0.058	0.329	”
0.607	0.074	0.042	0.277	”
0.603	0.076	0.045	0.276	”
0.606	0.074	0.043	0.277	”
0.557	0.076	0.054	0.313	”
0.606	0.074	0.046	0.274	”
0.488	0.087	0.067	0.359	[18]
0.58	0.074	0.054	0.292	[19]
0.544	0.075	0.063	0.318	”
0.577	0.074	0.057	0.292	”
0.59	0.07	0.05	0.29	[20]
0.568	0.078	0.057	0.297	[21]
0.563	0.079	0.057	0.301	[22]
0.57	0.078	0.057	0.295	[23]

5.3.3 Distances

Concerning the position of existing and future geoneutrino detectors we adopt the values used in [7]. The exact values of geographical coordinates (i.e. latitude and longitude) of nuclear power plants are not available on PRIS public database, since they are classified as sensitive information. In our calculation we adopt the positions of reactor cores as used in [7], according to Nasa Earth Observing System database [15], and we include the positions of most recent nuclear cores as available on Wikipedia. We calculate the distances by considering the Earth as an ellipsoid of revolution with equatorial radius a = 6378.388 km and a polar radius b = 6356.912 (see e.g. [16]). In order to take into account the signal uncertainty due to the distances, we compared the values of the signals, for the different geoneutrino experiments, obtained by assuming an ellipsoid with those obtained by assuming a spherical Earth (r=6371 km). We found variations less than 1%, see the fourth column of Table 5.5. It is interesting to note that the difference in the shape of the Earth practically does not affect the predicted reactor signal in SNO+, since almost one half of the signal is due to the near canadian nuclear plants.

5.4 Nuclear physics

The contribution to the reactor thermal power given by each fuel isotope depends on its specific fission fraction, discussed previously, as well as on the energy released per fission Q_i, i.e. the energy from the fission process of $i-th$ isotope that remains in the reactor core and it is transformed into heat .

As explained, for instance, in ref. [24], such energy is calculated starting from $(E_{tot})_i$, the total energy in fission from the instant at which the neutron, that induces fission of *i-th* isotope, is absorbed to the completion of the β decays of the product fragments and their transformation into β-stable atoms. It includes the total kinetic energy of the fission fragments, the total kinetic energy of the emitted prompt and delayed neutrons, and all the kinetic energy of the emitted photons, β particles and antineutrinos. Consequently the energy released per fission which remains in the reactor core is calculated as follows:

$$Q_i = (E_{tot})_i - \langle E_{\bar{\nu}} \rangle_i - (\Delta E_{\beta\gamma})_i + (E_{nc})_i \qquad (5.7)$$

where $\langle E_{\bar{\nu}} \rangle$ is the mean energy carried away by antineutrinos produced in the beta decays of fission fragments; $\Delta E_{\beta\gamma}$ is the energy of beta electrons and photons coming from fission fractions that do not decay and so does not contribute to the reactor energy during the operation of the core; E_{nc} is the energy released in neutron capture (without fission) by various materials of the reactor core.

In Table 5.2 we list the most recent values for Q_i adopted in our calculation. The effect of the uncertainties of Q_i on the predicted signal has been evaluated in the following way: we calculate *UP* and *DOWN* signals corresponding to the values $Q_i + \Delta Q_i$ and $Q_i - \Delta Q_i$ respectively, than we calculate the relative variation $|UP - DOWN|/(\sqrt{12} \cdot MEAN)$. The effect for different locations of geoneutrino experiments is reported in the 5th column of Tables 5.5 and 5.6.

Table 5.2 Energy released per fission, Q_i for the four isotopes involved in nuclear reactor process, from [24].

	^{235}U	^{238}U	^{239}Pu	^{241}Pu
Q_i [MeV]	202.36 ± 0.26	205.99 ± 0.52	211.12 ± 0.34	214.26 ± 0.33

5.4.1 Emitted antineutrino spectrum

The distribution of the fission products of uranium or plutonium involves hundreds of nuclei, each of them contributing to antineutrino emission spectrum. Thus, the total emitted antineutrino spectrum is the result of the sum of thousands of beta branches, weighted by the branching ratio of each transition and by the fission yield of the parent nucleus. The two traditional ways for predicting the total antineutrino

spectrum are the summation and the conversion methods. The summation procedure reconstructs the beta spectra using available nuclear databases as the sum of the branch-level beta spectra of all the daughter isotopes and then converts the beta spectra in antineutrino spectra. The conversion technique relies on direct measurements of the beta spectra and exploits the energy conservation law between the two leptons involved in the beta minus decay.

Starting from '80s several measurements of the total beta spectra of fissile isotopes have been performed, since these spectra act as benchmarks for the summation calculations and are direct inputs for the conversion method. In particular target foils of ^{235}U, ^{239}Pu and ^{241}Pu were exposed to an intense thermal neutron flux and the beta spectra of the unstable fragments were measured, see e.g. [25]. As ^{238}U undergoes fission when hit by fast neutrons, its beta spectrum could not be measured in the thermal flux.

Usually, for each isotope, the emitted antineutrino spectrum, normalized to one fission, is parameterized as follows:

$$\lambda_i(E_{\bar{\nu}}) = \exp\left(\sum_{p=1}^{n}(a_p)_i\, E_{\bar{\nu}}^{p-1}\right) \quad . \tag{5.8}$$

Along the years, in the literature several sets of polynomial coefficients have been presented, for different values for n, see e.g. [26, 27, 28]. In our calculation we adopt the most recent results by [28], where the spectra of all four contributing isotopes are consistently given in terms of the exponential of a polynomial of order 5, see Table 5.3. The authors derive the ^{235}U, ^{239}Pu and ^{241}Pu spectra based on a mixed approach that combines the accurate reference of measured electron spectra with the physical distribution of beta branches provided by the nuclear databases, and calculate the ^{238}U spectrum via a pure summation method.

Table 5.3 Coefficients entering in the parameterization of antineutrino spectra (Eq. 5.8), originating by the fission of the the isotopes mainly involved in the nuclear reactor process, from [28].

	^{235}U	^{238}U	^{239}Pu	^{241}Pu
a_1	3.217	4.833E-01	6.413	3.251
a_2	-3.111	1.927E-01	-7.432	-3.204
a_3	1.395	-1.283E-01	3.535	1.428
a_4	-3.690E-01	-6.762E-03	-8.820E-01	-3.675E-01
a_5	4.445E-02	2.233E-03	1.025E-01	4.254E-02
a_6	-2.053E-03	-1.536E-04	-4.550E-03	-1.896E-03

With a conservative attitude, in order to estimate the contribution to the signal error due to emitted antineutrino spectrum, we made a comparison between the signal obtained by using the most recent parameterization of ref. [28] with the signal obtained with the previous parameterization presented in ref.[27]. We found a difference of the order of 3%, see Table 5.5 and 5.6, in agreement with the fact that the shapes of the spectra obtained in the two references are comparable, whereas the

normalization is shifted by about +3% on average [28]. Such disagreement in the calculated emitted antineutrino spectra is an open question of the last few years, the so called 'reactor antineutrino anomaly', see e.g. [29].

5.5 Neutrino oscillation and neutrino detection

Reactor antineutrino signal at the detector site, depends obviously on the cross section of the reaction exploited for the detection and consequently on the flavour of the neutrinos coming into the detector.

5.5.1 Oscillation parameters

At present, most experimental results on neutrino flavour oscillation agree with a three neutrino scenario, where weak neutrino eigenstates, i.e. flavour eigenstates $(\nu_e, \nu_\mu, \nu_\tau)$ mix with the mass eigenstates (ν_1, ν_2, ν_3) via three mixing angles $(\theta_{12}, \theta_{13}, \theta_{23})$ and a possible CP-violating phase δ. Therefore, to establish the reactor antineutrino signal at a given site, it is necessary to consider the survival probability of the electron antineutrino, which can be expressed (assuming antineutrinos propagate in vacuum) in terms of the mass-mixing oscillation parameters $(\delta m^2, \theta_{12}, \theta_{13})$ as stated in [30]:

$$P_{ee}(E_{\bar{\nu}}, L) = cos^4(\theta_{13}) \left(1 - sin^2(2\theta_{12}) sin^2 \left(\frac{\delta m^2 L}{4E_{\bar{\nu}}} \right) \right) + sin^4(\theta_{13}) \quad , \qquad (5.9)$$

where δm^2 is the difference between the squared masses of mass eigenstates ν_1 and ν_2; L is the antineutrino path length; $E_{\bar{\nu}}$ is the antineutrino energy (all in natural units). In our calculation we adopt the updated values on neutrino oscillation parameters, obtained by [31] from a global fit to data provided by different experiments. At 1σ level these parameters are, for the case of Normal Hierarchy:

$$\delta m^2 = (7.54^{+0.26}_{-0.22}) \cdot 10^{-5} \, \text{eV}^2$$
$$sin^2\theta_{12} = 0.308 \pm 0.017$$
$$sin^2\theta_{13} = 0.0234^{+0.022}_{-0.018} \quad . \qquad (5.10)$$

The effect of oscillation parameters on error budget, was derived as follows. We vary the oscillation parameters one at a time, we calculate the UP (DOWN) signal corresponding to the increased (diminished) value of the parameter by the quantity equal to its 1σ error, then we calculate the relative variation of the signal as $|UP - DOWN|/(\sqrt{12} \cdot MEAN)$, i.e. we assume that the obtained signals follow an uniform distribution. The results, reported in Table 5.5 and 5.6, show that at the moment the major source of uncertainty is θ_{12} the mixing angle.

Note that the equation of survival probability adopted by us is valid for distance reactor-detector larger than 50 km, as it holds in our calculations; it is insensitive to the difference between the squared masses of mass eigenstates v_1-v_3 and v_2-v_3, so our result does not change if we consider the Inverted Hierarchy scenario. Clearly the situation changes when the distances become smaller or of the order of 50 km: the exact expression for the survival probability must be used (see e.g. [32]), and consequently the difference between normal and inverted hierarchy is relevant. This will be the case of JUNO experiment when the near nuclear plants will be fully operational.

5.5.2 Cross section

Finally, in order to determine the predicted signal, it is necessary to account for the detection process via the inverse beta reaction on free protons, see Eq. 5.1. As clearly stated in [33] such reaction appears really suitable in antineutrino detection (at sub-GeV) due to several reasons: the cross section is relatively large ($\sim 10^{-42}$cm^2), has a low threshold and can be accurately computed; the measurable positron energy is strongly correlated with the antineutrino energy; materials rich in free protons are relatively cheap (water and hydrocarbons); it is possible to reduce the background by using the space and time correlation between the prompt positron annihilation signal and the delayed neutron capture signal. In our calculation, we adopt the parameterization of the reaction cross section given by [33]:

$$\sigma(E_{\bar{v}}) = 10^{-43} cm^2 p_e E_e E_{\bar{v}}^{-0.07056+0.02018 ln E_{\bar{v}} - 0.001953 ln^3 E_{\bar{v}}} \tag{5.11}$$

where $E_e = E_{\bar{v}} - \Delta$ is the positron energy, $\Delta = m_n - m_p \approx 1.293$ MeV, $p_e = \sqrt{E_e^2 - m_e^2}$ is the positron momentum, $m_e = 0.511$ MeV is the positron mass. In the paper [33] the cross section has been analytically calculated, and the authors claim that parameterization of Eq. (5.11) agrees with their analytical result within few per mil for $E_{\bar{v}}$ up to 300 MeV. In addition, they observe that at low energy the cross section has an overall 0.4% uncertainty, due to the uncertainties on the input quantities used in the analytical estimate. Conservatively, we adopt a 0.4% constant contribution to the error in the signal determination because of inverse beta reaction cross section.

5.6 Other effects

It is worth mentioning some effects which were note taken into account in our calculation.

- *Spent nuclear fuel (SNF)*. In addition to short lived fission products discussed in section 5.3, there are other long lived isotopes, which are part of exhausted fuel, whose decays ($\tau \sim 300$ days or greater) give additional contribution to reactor antineutrino signal. This contribution is hard to estimate, since it depends on how and where the spent fuel is stored. It is normally kept in water pools in interim storages situated near nuclear power plants, but permanent waste storage are under construction, e.g. in Finland [34]. The KamLAND collaboration estimates that spent fuel provides an additional contribution of 2.4% to reactor antineutrino signal [1]. For the Chooz experiment, an increase of about 1.5% in the low energy region of the reactor antineutrino spectrum has been estimated in ref. [35], whereas the contribution of antineutrinos emitted from SNF determines a variation of +1.9% in the signal for the DayaBay detector [36].
- *Matter effect*. During their travel from reactors to detectors, neutrinos can interact with the matter in the Earth. So the survival probability discussed in section 5 is not strictly correct, since it refers to neutrino oscillation in vacuum. We investigated the matter effect by considering the Earth density profile as published in [37]. We found that, for the experimental sites we considered and for the nuclear reactors operating in year 2013, the contribution is at most +0.8%. Note that if we assume a homogeneous Earth with density ~ 12 g/cm^3 (a typical terrestrial core density !), we found out that, the matter effect gives an increase of about 3% in the calculated signal.
- *Other man-made antineutrino sources*. In our calculation, as already stated, we considered all operating commercial reactors in the world, and we do not take into experimental and military reactors due to their small thermal power (1-100 MW). Concerning nuclear propulsion adopted in marine transport, aircraft carriers and ice breakers can be equipped with nuclear reactors producing up to 300 MWth, these sources of antineutrinos must be taken into account for a geoneutrino detector placed near a harbour.

One can see that, at the moment, such effects are smaller than the total uncertainty on reactor antineutrino signals, quoted in Table 5.5 and 5.6. In the future, a more refined analysis could be useful.

5.7 Results and conclusions

In Fig. 5.3 we show the contribution of reactor antineutrino signal all over the world, as derived in the calculation discussed in sections above in the total energy window (1.8-10 MeV). Clearly, a geoneutrino detector eventually placed in the Central Europe, or in oriental part of USA as well as in Korea, is, at the moment, completely obscured by reactor antineutrino signal. Note how Laboratori Nazionali del Gran Sasso (LNGS) in Italy and Sudbury (in Canada) are at the borderline of the reactor antineutrino 'clouds'. Note that after the Fukushima's episode, reactor antineutrinos are almost completely absent in Japan. The same map reported several years ago in ref. [7] showed a completely different situation. We want to emphasize that a map

of reactor antineutrino signal cannot be considered definite at all, but it must be updated taking into account the continuously varying number of operating reactor nuclear plants in the world. On this respect an interesting project is discussed in ref. [9].
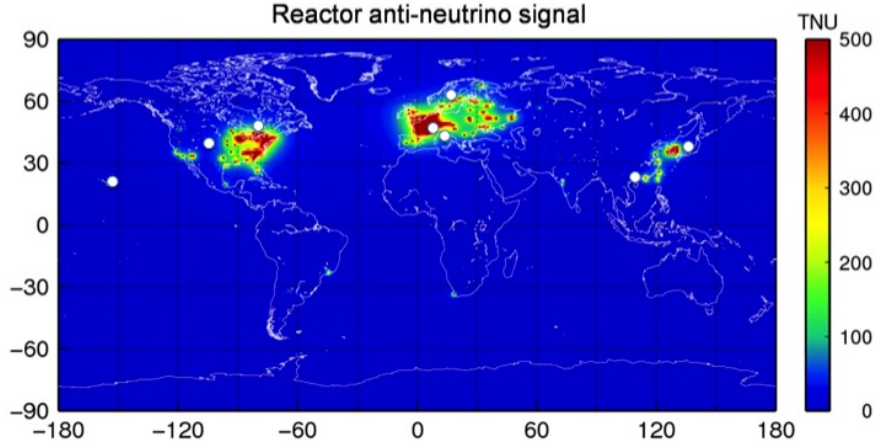
Fig. 5.3 A worldwide map of reactor antineutrinos signal, in the total energy window ($1.8 < E_{\bar{\nu}} < 10$ MeV). 1 TNU = 1event/year/10^{32} protons. The white dots indicate the positions of the operating and planned geoneutrino experiments, see Table 5.4 .

Table 5.4 Comparison between expected reactor (R) and geo (G) antineutrino signals. R_G indicates the reactor signals expected in the geo neutrino energy window ($1.8 < E_{\bar{\nu}} < 3.27$ MeV). Geoneutrino signal has been taken from [8], except for JIANGMEN which is from [9]. 1 TNU = 1event/year/10^{32} protons.

Sites	R [TNU]	R_G [TNU]	G [TNU]	R_G/G
LNGS (Italy)	84.7 ± 3.7	22.6 ± 0.84	$40.3^{+7.3}_{-5.8}$	0.6
KAMIOKA (Japan)	64.4 ± 2.8	18.3 ± 0.73	$31.5^{+4.9}_{-4.1}$	0.6
SUDBURY (Canada)	173.1 ± 7.0	42.9 ± 1.55	$45.4^{+7.5}_{-6.3}$	0.9
PHYASALMI (Finland)	66.8 ± 2.9	17.0 ± 0.63	$45.3^{+7.0}_{-5.9}$	0.4
FREJUS (France)	557.4 ± 24.0	129.3 ± 5.09	$42.4^{+7.6}_{-6.2}$	3.0
HOMESTAKE (USA)	27.3 ± 1.2	7.17 ± 0.26	$48.7^{+8.4}_{-6.9}$	0.1
HAWAII (USA)	3.36 ± 0.14	0.89 ± 0.03	$12.0^{+0.7}_{-0.6}$	0.1
JIANGMEN (China)	96.5 ± 4.1	26.7 ± 1.52	$39.7^{+6.5}_{-5.1}$	0.7

Now, let us focus our attention to some peculiar zones of the Earth. In Table 5.4, for a selected sample of geographical sites, we indicate the reactor antineutrino signal, both in the total energy window (1.8 -10 MeV) and in the geoneutrino energy window (1.8 -3.27 MeV), indicated as R and R_G respectively. In the same table we also report G, the predicted geoneutrinos signals as calculated in [8]. As already

stated in [7], the ratio R$_G$/G can be considered as a figure of merit for assessing the discrimination power on geoneutrinos at a specific location.

In the underground Laboratori Nazionali del Gran Sasso (LNGS) the Borexino detector has already measured a geoneutrino signal. The Kamioka mine, in Japan, is the site of KamLAND experiment which firstly asserted the observation of geoneutrinos. We observe that, until all the Japanese reactors will remained turned off, Kamioka is a suitable site for detecting geoneutrinos, comparable to LNGS.

In the near future, the SNO+ [3] experiment, in Sudbury mine in Canada, with a quite reasonable ratio R$_G$/G, will provide additional information about Earth's interior .

Concerning LENA project [4], a new European geoneutrino detector located at Frejus Laboratory would require a detailed knowledge of closeby reactors in order to provide useful data on geoneutrinos; the choice of Phyasalmi looks really better in this respect.

Of course Hawaii is a wonderful place for geoneutrino studies due to its position far away from any nuclear plant [5]. The same holds for Homestake, a mine in the United States where the Devis' s pioneering experiment on solar neutrino detection was located and that could became the site for a new underground laboratory [38].

The site for the future JUNO experiment, in China, planned to start data taking in 2020, is of some interest. When the close ($L \sim 53$ km) nuclear plants of Yangjiang and Taishan will become fully operational, the reactor antineutrino signal will increase enormously (about 1600 TNU), but due to the large detector mass (20 kton) one can obtain interesting values of geoneutrinos measurements during the periods of reactor technical shut down, see e.g. [39].

In Table 5.5 and 5.6 we report the contributions to the total error, arising from the different input data discussed in sections 3-5. One can see that the error budget is significantly dominated by the uncertainty on emitted antineutrino spectra. Note also that precise predictions of the antineutrino spectra emitted by nuclear reactors is a key ingredient in measurements of reactor neutrino oscillations, see e.g. [6], so refinements in the measurements and in the calculation are surely upcoming.

Concerning the neutrino oscillation parameters, the major contribution arises from the mixing angle θ_{12} and in the geoneutrino energy window also the contribution of δm^2 increases (for JUNO site it is really dominant). The effect of δm^2 parameter is strictly related to neutrino energy and to the reactor-detector distance since all these quantities appear in the oscillation phase, see Eq. 5.9. Future experiments are planned also for precision measurement of neutrino mixing parameters (see e.g. [6]).

It is worth observing that, in this work, we have made several important assumptions in performing error estimates: we assume a constant uncertainty for the thermal power in order to include also our limited knowledge on the thermal Load Factor of each core; we probably overestimate the uncertainty related to emitted antineutrino spectra $\lambda_i(E_{\bar{v}})$; we assume that the different signals, obtained by varying each parameters at time, follow a uniform distribution; finally we considered all sources of uncertainties completely uncorrelated. A further treatment of uncertainties, based on a MonteCarlo method, is performed in [9].

Table 5.5 For different geographical sites we report the relative contributions (in %) to the total error in the calculated reactor antineutrino signals, due to the different input data used in the calculation. We consider here the total energy window of reactor antineutrinos (1.8 -10 MeV). The values of column TOTAL have been calculated as the square root of the sum of the squares of the various contributes. For the definition of the parameters indicated in the first row of the table see text.

sites	P_r	f_i	L_r	Q_i	λ_i	σ	δm^2	$sin^2\theta_{12}$	$sin^2\theta_{13}$	TOTAL
LNGS	2.0	0.83	0.27	0.09	3.5	0.4	0.02	1.31	0.23	4.3
KAMIOKA	2.0	0.92	0.31	0.09	3.4	0.4	0.44	1.19	0.23	4.3
SUDBURY	2.0	0.44	0.04	0.09	3.2	0.4	0.01	1.34	0.23	4.1
PHYASALMI	2.0	0.89	0.50	0.09	3.4	0.4	0.04	1.31	0.23	4.3
FREJUS	2.0	0.87	0.37	0.09	3.6	0.4	0.08	1.13	0.23	4.4
HOMESTAKE	2.0	0.84	0.37	0.09	3.4	0.4	0.004	1.31	0.23	4.3
HAWAII	2.0	0.84	0.32	0.09	3.4	0.4	<0.001	1.31	0.23	4.3
JIANGMEN	2.0	0.94	0.27	0.09	3.4	0.4	0.54	1.31	0.23	4.3

Table 5.6 The same as in Table 5.5, but calculated by considering the reactor antineutrino signal in the geoneutrino energy window.

sites	P_r	f_i	L_r	Q_i	λ_i	σ	δm^2	$sin^2\theta_{12}$	$sin^2\theta_{13}$	TOTAL
LNGS	2.0	0.56	0.38	0.09	2.6	0.40	0.76	1.29	0.23	3.7
KAMIOKA	2.0	0.59	0.14	0.09	2.6	0.40	1.88	0.98	0.23	4.0
SUDBURY	2.0	0.32	< 0.001	0.08	2.5	0.40	0.39	1.59	0.23	3.6
PHYASALMI	2.0	0.60	0.49	0.09	2.6	0.40	0.07	1.43	0.23	3.7
FREJUS	2.0	0.57	0.19	0.09	2.6	0.40	1.34	1.53	0.23	3.9
HOMESTAKE	2.0	0.57	0.53	0.09	2.6	0.40	0.04	1.33	0.23	3.7
HAWAII	2.0	0.57	0.37	0.09	2.6	0.40	0.01	1.31	0.23	3.6
JIANGMEN	2.0	0.62	0.56	0.09	2.7	0.40	4.32	1.16	0.23	5.7

References

1. T. Araki et al. (KamLAND Collaboration), Nature **436** 499 (2005); A. Gando et al. (KamLAND Collaboration), Nature Geoscience **4**, 647 (2011); A. Gando et al. (KamLAND Collaboration), Physical Review D **88**, 033001 (2013).
2. G. Bellini et al. (Borexino Collaboration), Phys. Lett. B **687**, 299 (2010); G. Bellini et al. (Borexino Collaboration), Phys. Lett. B **722**, 295 (2013).
3. SNO+ Collaboration: C. Kraus et al. Prog. Part. Nucl. Phys. **57**, 150 (2006); M. Chen et al., Earth, Moon, and Planets **99**, 221 (2006).
4. M. Wurm et al. Astrop.Phys. **35**, 685 (2012).
5. S. T. Dye et al., Earth Moon Planets **99**, 241 (2006) .
6. Y.-F. Li, International Journal of Modern Physics: Con- ference Series **31**, 1460300 (2014).
7. G. Fiorentini, M.Lissia and F. Mantovani, Phys. Rep. **453**, 117 (2007).
8. B. Ricci et al, PoS(Neutel 2013) **077**, 382 (2014), Proceedings of XV Workshop on Neutrino Telescopes, 11-15 March 2013, Venice, Italy.
9. M. Baldoncini et al. (2014), in preparation.
10. International Nuclear Safety Center at Argonne National Laboratory, 2005 database, `http://insc.ans.org`.
11. IAEA-PRIS, The Database on Nuclear Power Ractors, `http://www.iaea.org/PRIS/home.aspx`.
12. J. Mandula, Nuclear Power Engeneering Section, IAEA-PRIS database 2013.
13. Z. Djurcic et al , Journal of Physics G: Nuclear and Particle Physics **36**, 045002 (2009).
14. K.S. Krane: Introductory Nuclear Physics, John Wiley & Sons Inc. New York, 1988, ISBN 0-471-80553-X.
15. Nasas Earth Observing System, Data and Information system, `http://gcmd.nasa.gov` (2006).
16. Mean Earth ellipsoid and Reference ellipsoids, `http://en.wikipedia.org/wiki/Earth_ellipsoid`.
17. G. Mention et al, Physical Review D **83**, 073006 (2011).
18. Y. Abe et al. (Double Chooz Collaboration), Physical Review Letters **108**, 131801 (2012).
19. Z. Djurcic et al, Journal of Physics G: Nuclear and Particle Physics **36**, 045002 (2009).
20. V. I. Kopeikin, L. A. Mikaelyan, and V. V. Sinev, Physics of Atomic Nuclei **67**, 1892 (2004).
21. K. Eguchi et al. (KamLAND Collaboration), Physical Review Letters **90**, 021802 (2003).
22. T. Araki et al. (KamLAND Collaboration), Physical Review Letters **94**, 081801 (2005).
23. S. Abe et al. (KamLAND Collaboration), Physical Re- view Letters **100**, 221803 (2008).
24. X. B. Ma et al, Physical Review C **88**, 014605 (2013).
25. K. Schreckenbach et al, Physics Letters B **160**, 325 (1985).
26. P. Vogel, Physical Review C **76**, 025504 (2007).
27. P. Huber and T. Schwetz, Phys. Rev. D **70**, 053011 (2004).
28. Th. A. Mueller et al., Phys. Rev. C **83**, 054615 (2011).
29. G. Mention et al, Phys. Rev. D **83**, 073006 (2011).
30. G. Fiorentini et al., Phys. Rev. D **86**, 033004 (2012).
31. F. Capozzi et al, Phys. Rev. D **89**, 093018 (2014)
32. F. Capozzi, E. Lisi and and A. Marrone, Phys. Rev. D **89**, 013001 (2014).
33. A. Strumia and F. Vissani, Phys. Lett. B **564**, 42 (2003).
34. Nuclear Waste Management in Finland; `http://www.energia.fi/en/publications/nuclear%20waste.pdf`.
35. V. I. Kopeikin, L. A. Mikaelyan, and V. V. Sinev, Physics of Atomic Nuclei **69**, 185 (2006).
36. Z. Bin et al. Chinese Physics C **36**, 1 (2012).
37. A. M. Dziewonski and D. L. Anderson, Phys. Earth Planet. Interiors **25**, 297 (1981).
38. Deep Underground Science and Engineering Laboratory (DUSEL), `http://www.int.washington.edu/DUSEL/homestake.html`.
39. V. Strati et al in preparation (2014).